Received 12 August 2021; revised 4 October 2021; accepted 24 October 2021. Date of publication 1 November 2021; date of current version 10 November 2021. The review of this article was arranged by Editor M. J. Kumar

Digital Object Identifier 10.1109/JEDS.2021.3124327

An Intrinsic Small-Signal Equivalent Circuit Model for AlGaN/GaN HEMT Considering the Momentum Balance Equation

Y. PEI[1] (Senior Member, IEEE), AMGAD A. AL-SAMAN[1,2], CHENGONG YIN[1], EUGENY A. RYNDIN[3], AND FUJIANG LIN[2] (Senior Member, IEEE)

1 Device Technology Department, Dynax Semiconductor Inc., Suzhou 215300, China
2 School of Microelectronics, University of Science and Technology of China, Hefei 230026, Anhui, China
3 Department of Micro- and Nanoelectronics, Saint Petersburg Electrotechnical University "LETI", 197376 Saint Petersburg, Russia

CORRESPONDING AUTHOR: Y. PEI (e-mail: yi.pei@dynax-semi.com)

This work was supported by the National Key Research and Development Program of China under Grant 2019YFB2204601.

ABSTRACT High-frequency dispersion of the AlGaN/GaN HEMT output resistance has been investigated. Using the electron momentum balance equation, we demonstrated that the deviation of the dynamic drift velocity from its static value could be considered as the main reason for the high-frequency dispersion of the transistor output resistance. Moreover, a new intrinsic small-signal equivalent circuit has been proposed to consider the output resistance dispersion. Comparison with measured s- parameters have validated the proposed approach.

INDEX TERMS Gallium nitride, high electron mobility transistors, frequency dispersion, small-signal model.

I. INTRODUCTION

The small-signal modeling of microwave GaN HEMT devices is a research topic of high importance in microwave circuit design and device characterization [1], [2]. The small-signal model is required to reproduce the GaN HEMT transistor behavior, and it is considered as the first step to developing the large-signal and noise models [3]–[5]. Currently, two approaches of small-signal modelling coexist: 1) the electrical approach, which is based on the equivalent circuit models, and 2) the behavioral approach, which is based on the artificial neural networks (ANNs) [3]. Even though the behavioral approach gives an accurate reproducing of the S-parameters measurement, it has no connection with device physics and circuitry. Mainly this makes such models less preferable for RF and microwave designers.

A preferable approach for the RF and microwave designers is the electrical approach. It is based on the equivalent circuits that commonly consist of an extrinsic part representing the parasitic elements and an intrinsic part representing the bias-depending elements. Several approaches, extraction methodology, and optimization algorithms have been developed seeking for high accuracy value of extracted parameters during the past decades [6]–[9]. Away from the optimization and extracting procedure, any small-signal model's core is the equivalent circuit used to represent the GaN/AlGaN HEMT. Several attempts have been made to modify the equivalent circuit of the GaN HEMT; however, most of them are related to the extrinsic part of the equivalent circuit. For example, in [10], the author proposed a new modified equivalent circuit that contains 20 elements. However, the modifications attach only the extrinsic part of the device, where the author tried to consider parasitic capacitances of the pads and inter-electrode/crossover separately. Despite the good fit achieved by [10] with measured S_{11}, S_{12}, and S_{21}–parameters, a pretty poor fit with S_{22} -parameter, especially at relatively high frequency. The frequency dispersion in GaN has been given great attention as the mechanism responsible for the device degradation. In [11], the frequency dispersion was modeled using an additional circuit with a delay time of around 1 microsecond. However, the model can capture the dispersion effect due to the trapping and de-trapping up to 1 GHz. This can not explain the dispersion of S_{22} -parameter at high frequency. The agreement with S_{22} -parameter is crucially important for circuit design as it determines the output impedance of the HEMT transistor and, as a consequence, the matching quality. At MIMC design, especially at high frequency or mm-wave, the matching itself becomes an issue, and any inaccuracy of the modeled S_{22} may lead to poor output performance of the design. To overcome such difficulties and physically explain such high-frequency dispersion, the equivalent circuit's intrinsic part will be investigated.

II. MODEL DESCRIPTION

The intrinsic part of the small-signal circuit should represent the active region of the HEMT transistor. For this reason, it should replicate the main physical phenomena within the active region [12]. In other words, each element of the intrinsic circuit should be linked to the device's physics. Traditionally, the intrinsic part of the small-signal model believed to be frequency independent and built assuming stationary transport of the electrons where is the time-dependence of the drift velocity and energy have been neglected. Such an assumption can be valid for relatively low frequency. However, while moving toward a high-frequency range, the time-dependence of drift velocity should be taken into account. Let us assume that the electrical field consists of two components, one resulting from time-independent bias E_0 and another from the time-dependent applied signal $\widetilde{E} = 2E_1 \cos(\omega t)$, so:

$$E(t) = E_0 + 2E_1 \cos(\omega t) \tag{1}$$

where $2E_1$ is the magnitude of the electrical field of the RF signal, ω is the cyclic frequency of the applied RF signal, and E_0 is the electrical field due to DC applied voltage.

The simplified momentum balance equation can be written as [13]–[16]:

$$\frac{\partial P(t)}{\partial t} = -qE(t) - \frac{P(t)}{\langle \tau_m \rangle} \tag{2}$$

where $P(t)$ is the electron momentum, q is the elementary charge, and $\langle \tau_m \rangle$ is the averaged momentum relaxation time, usually defined at the condition $\partial P/\partial t = 0$. While deriving equation (2), we have assumed that the concentration gradients' effect on the electron momentum is negligible. The electron momentum related to the drift velocity within the classical approach by [16]:

$$P(t) = m^* v(t) \tag{3}$$

where m^* is the electron effective mass, $v(t)$ is the drift velocity of the electrons.

Assuming that the effective mass is time-independent, the equation 1 with accounting for equation (3) can be rewritten [16]:

$$\frac{\partial v(t)}{\partial t} = -\frac{q}{m^*} E(t) - \frac{v(t)}{\langle \tau_m \rangle}. \tag{4}$$

For a small-signal and diminish magnetic field, the drift velocity will oscillate with a small amplitude at the driven frequency so that one may write [17]:

TABLE 1. SSM parameters at three bias conditions.

Bias Condition	C_{gs}(fF)	C_{ds}(fF)	R_{ds}(ohm)	gm(mS)	R_ω(ohm)
V_d=20V I_d=393mA	6042	1088	66	762	3.7
V_d=20V I_d=179mA	5227	991	71	605	2.7
V_d=20V I_d=83mA	4219	883	90	405	1.9

$$v(t) = v_0 + 2v_1 \cos(\omega t). \tag{5}$$

Applying equation (5), the equation (4) may be rewritten as:

$$\begin{aligned} \frac{\partial}{\partial t}[v_0 + 2v_1 \cos(\omega t)] &= \frac{\partial v_0}{\partial t} + 2\cos(\omega t)\frac{\partial v_1}{\partial t} \\ &\quad + 2v_1 \frac{\partial}{\partial t}[\cos(\omega t)] \\ &= -\frac{q}{m^*}E(t) - \frac{v(t)}{\langle \tau_m \rangle}. \end{aligned} \tag{6}$$

Multiplying both parts of equation (6) be the relaxation time one may obtain:

$$\begin{aligned} &\langle \tau_m \rangle \frac{\partial v_0}{\partial t} + 2\langle \tau_m \rangle \cos(\omega t)\frac{\partial v_1}{\partial t} - 2\langle \tau_m \rangle v_1 \omega \sin(\omega t) \\ &= -\frac{q\langle \tau_m \rangle}{m^*}E(t) - v(t). \end{aligned} \tag{7}$$

The momentum relaxation time related to the time-dependent electron mobility $\mu(t)$ by [13]–[15]:

$$\mu(t) = \frac{q\langle \tau_m \rangle}{m^*}. \tag{8}$$

The momentum relaxation time $\langle \tau_m \rangle$ depends on the electrical field and has value in the range of $10^{-9} \sim 10^{-12}$ s. At the same time, the maximum drift velocity that has been recorded for GaN is $v_{peak} \approx 2.7 \times 10^5$ m/s. Based on this, the first two terms on the left-hand side of the equation (7) can be neglected. Thus the equation (7) with account for equation (8) can be rewritten as:

$$v(t) = -\mu(t)E(t) + \frac{2v_1 m^* \omega}{q} \mu \sin(\omega t). \tag{9}$$

Equation (9) clearly shows that the drift velocity will deviate from the conventional value expressed in form $v(t) = -\mu(t)E(t)$. The amount of drift velocity deviation is linearly increasing as one moves toward a higher frequency.

The electron mobility can be written as a function of the electrical field using [13]:

$$\mu(t) = \frac{\mu_L(T)}{\left(1 + (E(t)/E_c(T))^\beta\right)^{1/\beta}} \tag{10}$$

where $\mu_L(T)$ and $E_c(T)$ are the low-field electron mobility and critical electrical field of the channel layer as a function of the lattice temperature, and $\beta > 1$ for GaN.

Substituting equation (1) into equation (10), one may obtain:

$$\mu(t) = \frac{\mu_L(T)}{\left(1+\left(\frac{E_0+2E_1\cos(\omega t)}{E_c(T)}\right)^{\beta}\right)^{1/\beta}} = \frac{\mu_L(T)}{\left(1+\left(\frac{E_0}{E_c(T)}+\frac{2E_1\cos(\omega t)}{E_c(T)}\right)^{\beta}\right)^{1/\beta}}. \tag{11}$$

For small-signal excitation the $2E_1 << E_c(T)$ and $|\cos(\omega t)| \leq 1$ correspondingly, the following inequalities take place:

$$\left|\frac{2E_1\cos(\omega t)}{E_c(T)}\right| << 1 \tag{12}$$

$$\left|\frac{2E_1\cos(\omega t)}{E_c(T)}\right| << \frac{E_0}{E_c(T)}. \tag{13}$$

Using (12) and (13), the equation for the electron mobility can be rewritten as follows:

$$\mu(t) \approx \frac{\mu_L(T)}{\left(1+\left(\frac{E_0}{E_c(T)}\right)^{\beta}\right)^{1/\beta}} = \mu. \tag{14}$$

From equation (14), the time dependence of mobility can be neglected. Therefore in further discussion, the mobility will be denoted simply by μ. Substituting equations (1) and (14) into equation (9), one may get the following:

$$v(t) = -\mu E_0 - 2\mu E_1\cos(\omega t) + \frac{2v_1 m^*\omega}{q}\mu\sin(\omega t). \tag{15}$$

Taking into account that $\sin(\omega t) = \cos(\omega t + \frac{\pi}{2})$ along with equation (15), the drift velocity can be presented as follows:

$$v(t) = -\mu E_0 - 2\mu E_1\cos(\omega t) + \frac{2v_1 m^*\omega}{q}\mu\cos\left(\omega t + \frac{\pi}{2}\right). \tag{16}$$

From equation (16), it is clear that the drift velocity has linear frequency-dependent terms with $\pi/2$ phase shift compared to the input signal. Assuming a small diffusion current, one may write the drain current as:

$$I(t) = -qWn_s v(t). \tag{17}$$

The negative sign in equation (17) indicates that the conditional positive current follow is opposite to the direction of the electron transport. Substituting equation (16) for drift velocity with account for equations (1), one may obtain:

$$\begin{aligned} I(t) &= -qWn_s\left(-\mu E_0 + \frac{2v_1 m^*\omega}{q}\mu\cos\left(\omega t+\frac{\pi}{2}\right) - 2\mu E_1\cos(\omega t)\right) \\ &= -qWn_s\left(-\mu E_0 + 2v_1\langle\tau_m\rangle\omega\cos\left(\omega t+\frac{\pi}{2}\right) - 2\mu E_1\cos(\omega t)\right). \end{aligned} \tag{18}$$

Rearranging the equation (18), following by integration over the channel length it can be rewritten as:

$$\begin{aligned} \int_0^{L_g} I(t)dx &= \mu qWn_s\int_0^{L_g} E_0 dx - 2qWn_s\langle\tau_m\rangle\mu\omega \\ &\times \cos\left(\omega t+\frac{\pi}{2}\right)\int_0^{L_g}\frac{v_1}{\mu}dx \\ &+ 2qWn_s\mu\cos(\omega t)\int_0^{L_g} E_1 dx. \end{aligned} \tag{19}$$

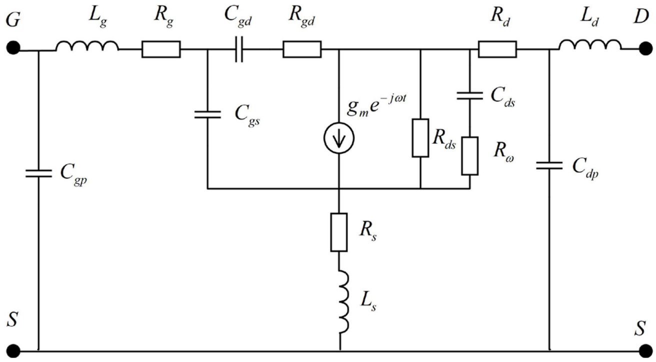

FIGURE 1. **The proposed small signal model.**

The current is constant throughout the channel length. Thus one may write:

$$\begin{aligned} I(t) = \underbrace{\frac{\mu qWn_s}{L_g}}_{G_{ds}}\underbrace{\int_0^{L_g} E_0 dx}_{\text{Voltage drop on } G_{ds}} - \underbrace{\frac{2qWn_s\langle\tau_m\rangle\mu\omega\cos\left(\omega t+\frac{\pi}{2}\right)}{L_g}}_{G_\omega} \\ \times \underbrace{\int_0^{L_g}\frac{v_1}{\mu}dx}_{\text{Voltage drop on } G_\omega} + \underbrace{\frac{2qWn_s\mu\cos(\omega t)}{L_g}}_{g_m}\underbrace{\int_0^{L_g} E_1 dx}_{\text{Voltage drop on } g_m} \end{aligned} \tag{20}$$

From equation (12), one may conclude that the dynamic nature of the physical process within the transistor, including the drift velocity, may lead to the transistor conductance's high-frequency dispersion. Therefore, the transistor output conductance/resistance can be divided into two parts: 1) frequency-independent output conductance/resistance G_{ds} (see equation (22)) and 2) frequency-dependent output conductance/ resistance G_ω. Therefore, the output resistance, frequency-dependent output resistance can be estimated using the following equations:

$$R_{ds} = \frac{L_g}{qW\mu n_s} \tag{21}$$

$$\begin{aligned} R_\omega &= \frac{L_g}{2qWn_s\mu\langle\tau_m\rangle\omega\cos\left(\omega t+\frac{\pi}{2}\right)} = \frac{R_{ds}}{2\langle\tau_m\rangle\omega\cos\left(\omega t+\frac{\pi}{2}\right)} \\ &= \frac{qR_{ds}}{2\mu m^*\omega\cos\left(\omega t+\frac{\pi}{2}\right)}. \end{aligned} \tag{22}$$

In addition, the current through frequency-dependent conductance/ resistance should be shifted by $\pi/2$. Based on the conclusions mentioned above, the intrinsic small-signal equivalent circuit should be modified by adding the effect of frequency dispersion. Fig. 1 describes the small-signal equivalent circuit, where the dispersion of the transistor conductance has been included by inserting a resistance R_ω in series with the source-drain capacitance.

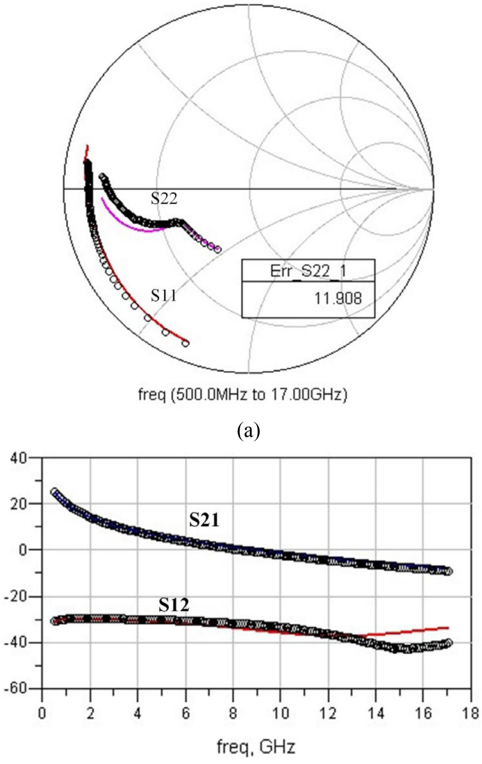

FIGURE 2. Comparison of S-parameters between experimental data (circle) and simulation data (line) by using the traditional model at Vd = 20V Id = 393mA (a) S11 and S22 (b) S21 and S12.

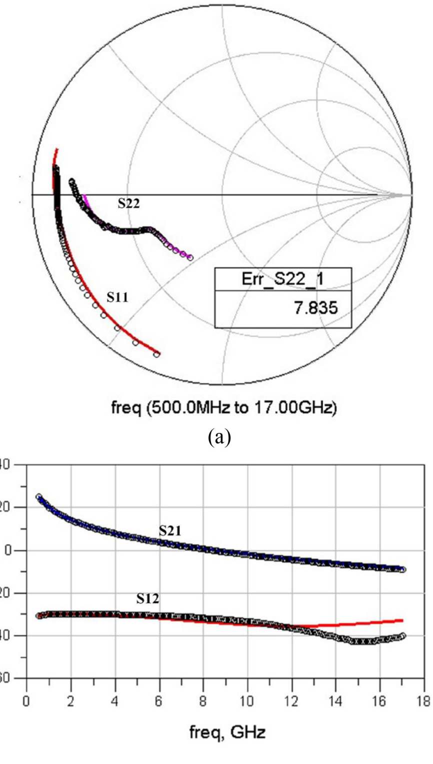

FIGURE 3. Comparison of S-parameters between experimental data (circle) and simulation data (line) by using the proposed model at Vd = 20V Id = 393mA (a) S11 and S22 (b) S21 and S12.

III. MODEL VALIDATION

To validate the findings, 2.1 mm gate-width AlGaN/GaN HEMT has been fabricated on a 3-in RF GaN-on-SiC process. First, to exclude the effect of extrinsic parasitic elements, open and short structures are used to de-embed extrinsic parameters (C_{pg}, C_{pd} L_g, L_d, and L_s). The gate, source, and drain resistances (R_g, R_d and R_s) are extracted using S- parameters at cold FET condition. The extrinsic parameters were accordingly optimized. Having excluded the effect of the extrinsic part of AlGaN/GaN HEMTs, the intrinsic parameters of the small-signal equivalent circuit can be easily extracted using measurement s-parameters at the hot FET condition.

To more clearly investigate the high-frequency dispersion of the channel resistance, we used two different small-signal intrinsic equivalent circuits: The first is the traditional equivalent circuit without the frequency-dependent resistance. The second is the proposed equivalent circuit with frequency-dependent resistance. The comparison between measured and simulated S-parameters using conventional and the proposed equivalent circuits has been performed over different currents and bias conditions. As shown from the comparison result for $V_d = 20V$, $V_d = 16V$, and $V_d = 12V$ correspondingly $I_d = 393mA$, $I_d = 392$ mA, and $I_d = 385mA$, the proposed model has an apparent advantage over the traditional one. Inserting the frequency-dependent resistance has reduced the averaged error of S_{22} by approximately 4% and error at a frequency higher than 6 GHz by more than 7% (See Fig. 2 to Fig. 7). Table 1 lists the SSM parameters at three bias conditions (different current and fixed drain voltage). It is worth noting that the frequency-dependent resistance R_ω has been averaged over the frequency range from 7 to 17 GHz and optimized. However, the averaging will not give as good a result as expected for a wider range, and the frequency dependence must be included.

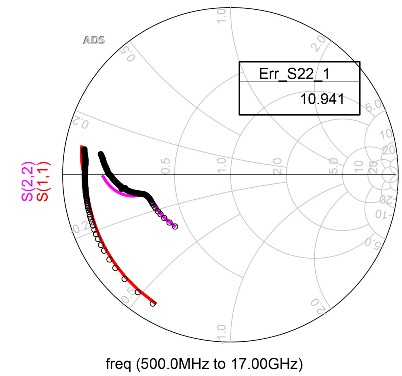

FIGURE 4. Comparison of S-parameters between experimental data (circle) and simulation data (line) by using the traditional model at Vd = 16V Id = 392 mA.

The frequency-dependent resistance R_ω is dependent on bias conditions as it depends on the mobility, electrical

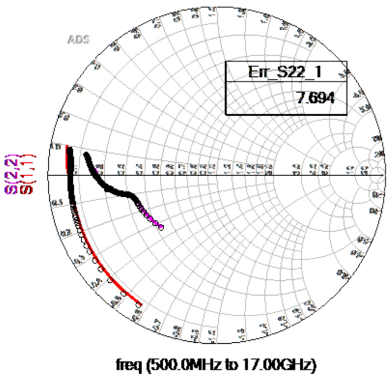

FIGURE 5. **Comparison of S-parameters between experimental data (circle) and simulation data (line) by using the proposed model at Vd = 16V Id = 392 mA.**

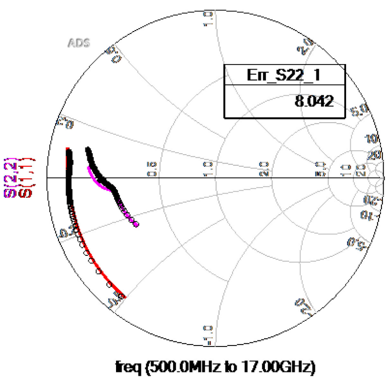

FIGURE 6. **Comparison of S-parameters between experimental data (circle) and simulation data (line) by using the traditional model at Vd = 12V Id = 385 mA.**

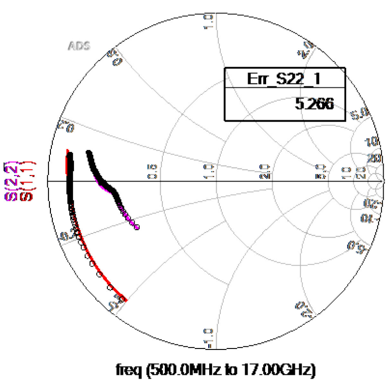

FIGURE 7. **Comparison of S-parameters between experimental data (circle) and simulation data (line) by using the proposed model at Vd = 12V Id = 385 mA.**

field, and electron concentration. Table 1 shows that with current decreasing caused by carrier concentration decrease due to the different gate voltage, the output resistance R_{ds} increase. However, the frequency-dependent R_ω declines. This decrease is related to two possible reasons. First, the term $\cos(\omega t+\pi/2)$, the time here, is the extracted time delay, increasing proportionally to the current. At low current, the time delay reduces, causing the cosine term to approach one $\cos(\omega t + \pi/2) = 1$. This, in turn, increases the conductance and reduces the corresponding resistance. Second, electron mobility may affect the frequency-dependent resistance. As seen from equation (22), the frequency-dependent resistance is inversely proportional to electron mobility. At the high current, the dissipation power increases propositionally. This, in turn, increase the channel and carrier temperature. The increase in the temperature sharply reduces the mobility and, as a consequence, increase the frequency-dependent output resistance. As it seen from the Table 1 the frequency-dependent resistance decreases with output power decreasing.

IV. CONCLUSION

A modified intrinsic small-signal equivalent circuit has been developed. The model considers the drift velocity nonlinearity and, as a consequence, the high-frequency dispersion of the channel resistance. Comparison with measured S-parameter shows that the consideration of channel resistance dispersion increases the model's accuracy by approximately 7% compared to traditional small-signal models.

REFERENCES

[1] G. Dambrine, A. Cappy, F. Heliodore, and E. Playez, "A new method for determining the FET small-signal equivalent circuit," *IEEE Trans. Microw. Theory Techn.*, vol. 36, no. 7, pp. 1151–1159, Jul. 1988, doi: 10.1109/22.3650.

[2] G. Crupi, A. Caddemi, D. M. M.-P. Schreurs, and G. Dambrine, "The large world of FET small-signal equivalent circuits," *Int. J. RF Microw. Comput.-Aided Eng.*, vol. 26, no. 9, pp. 749–762, Aug. 2016. [Online]. Available: https://doi.org/10.1002/mmce.21028

[3] Z. Marinković, G. Crupi, A. Caddemi, and V. Marković, "GaN HEMT small-signal modelling: Neural networks versus equivalent circuit," in *Proc. IEEE 30th Int. Conf. Microelectron. (MIEL)*, Nis, Serbia, 2017, pp. 153–156, doi: 10.1109/MIEL.2017.8190090.

[4] A. Raffo, V. Vadalà, G. Bosi, F. Trevisan, G. Avolio, and G. Vannini, "Waveform engineering: State-of-the-art and future trends," *Int. J. RF Microw. Comput.-Aided Eng.*, vol. 27, no. 1, Sep. 2017, Art. no. e21051. [Online]. Available: https://doi.org/10.1002/mmce.21051

[5] A. Nalli *et al.*, "GaN HEMT noise model based on electromagnetic simulations," *IEEE Trans. Microw. Theory Techn.*, vol. 63, no. 8, pp. 2498–2508, Aug. 2015, doi: 10.1109/TMTT.2015.2447542.

[6] Q. Fan, J. H. Leach, and H. Morkoc, "Small signal equivalent circuit modeling for AlGaN/GaN HFET: Hybrid extraction method for determining circuit elements of AlGaN/GaN HFET," *Proc. IEEE*, vol. 98, no. 7, pp. 1140–1150, Jul. 2010, doi: 10.1109/JPROC.2010.2044630.

[7] S. Nuttinck, E. Gebara, J. Laskar, J. Shealy, and M. Harris, "Improved RF modeling techniques for enhanced AlGaN/GaN HFETs," *IEEE Microw. Wireless Compon. Lett.*, vol. 13, no. 4, pp. 140–142, Apr. 2003, doi: 10.1109/LMWC.2003.811062.

[8] A. G. Avval and S. M. El-Ghazaly, "A new small-signal modelling approach for analyzing HEMTs over a broad frequency range," in *Proc. IEEE 62nd Int. Midwest Symp. Circuits Syst. (MWSCAS)*, Dallas, TX, USA, 2019, pp. 706–709, doi: 10.1109/MWSCAS.2019.8885200.

[9] A. Majumder, S. Chatterjee, S. Chatterjee, S. S. Chaudhari, and D. R. Poddar, "Optimization of small-signal model of GaN HEMT by using evolutionary algorithms," *IEEE Microw. Wireless Compon. Lett.*, vol. 27, no. 4, pp. 362–364, Apr. 2017, doi: 10.1109/LMWC.2017.2678437.

[10] Z. Wen, Y. Xu, C. Wang, X. Zhao, and R. Xu, "An efficient parameter extraction method for GaN HEMT small-signal equivalent circuit model," *Int. J. Numer. Model. Electron. Netw. Devices Fields*, vol. 30, no. 1, p. e2127, Dec. 2017. [Online]. Available: https://doi.org/10.1002/jnm.2127

[11] S. D. Nsele, L. Escotte, J.-G. Tartarin, S. Piotrowicz, and S. L. Delage, "Broadband frequency dispersion small-signal modeling of the output conductance and transconductance in AlInN/GaN HEMTs," *IEEE Trans. Electron Devices*, vol. 60, no. 4, pp. 1372–1378, Apr. 2013.

[12] R. G. Brady, C. H. Oxley, and T. J. Brazil, "An improved small-signal parameter-extraction algorithm for GaN HEMT devices," *IEEE Trans. Microw. Theory Techn.*, vol. 56, no. 7, pp. 1535–1544, Jul. 2008, doi: 10.1109/TMTT.2008.925212.

[13] D. Vasileska and S. M. Goodnick, "Computational electronics," in *Synthesis Lectures on Computational Electromagnetics*, vol. 1, no. 1, 1st ed. San Rafael, CA, USA: Morgan Claypool, 2006, pp. 1–216. [Online]. Available: https://doi.org/10.2200/S00026ED1V01Y200605CEM006

[14] A. Forghieri, R. Guerrieri, P. Ciampolini, A. Gnudi, M. Rudan, and G. Baccarani, "A new discretization strategy of the semiconductor equations comprising momentum and energy balance," *IEEE Trans. Comput.-Aided Design Integr. Circuits Syst.*, vol. 7, no. 2, pp. 231–242, Feb. 1988, doi: 10.1109/43.3153.

[15] M. S. Shur, *GaAs Devices and Circuits*, 3rd ed. New York, NY, USA: Springer, Jul. 1989, doi: 10.1007/978-1-4899-1989-2.

[16] J. Požela, *Physics of High-Speed Transistors*, 1st ed. New York, NY, USA: Springer, 1993, doi: 10.1007/978-1-4899-1242-8.

[17] E. Ryndin and A. Al-Saman, "A novel approach to model high-speed microelectronic switch on the basis of hydrodynamic approximation," in *Proc. SPIE Int. Conf. Micro Nano Electron.*, vol. 11022. Zvenigorod, Russia, 2018, Art. no. 110220J. [Online]. Available: https://doi.org/10.1117/12.2521711

[18] X. L. Lei and N. Horing, "Balance-equation approach to hot-carrier transport in semiconductors," in *Physics of Hot Electron Transport in Semiconductors* (Topics in Applied Physics), vol. 58. New York, NY, USA: Springer-Verlag, 1992, pp. 1–132. [Online]. Available: https://doi.org/10.1142/9789814354806_0001.